

Coffee Rings as Low-Resource Diagnostics: Detection of the Malaria Biomarker *Plasmodium falciparum* Histidine-Rich Protein-II Using a Surface-Coupled Ring of Ni(II)NTA Gold-Plated Polystyrene Particles

Christopher P. Gulka,[†] Joshua D. Swartz,[†] Joshua R. Trantum,[‡] Keersten M. Davis,[†] Corey M. Peak,[‡] Alexander J. Denton,[†] Frederick R. Haselton,^{*,‡} and David W. Wright^{*,†}

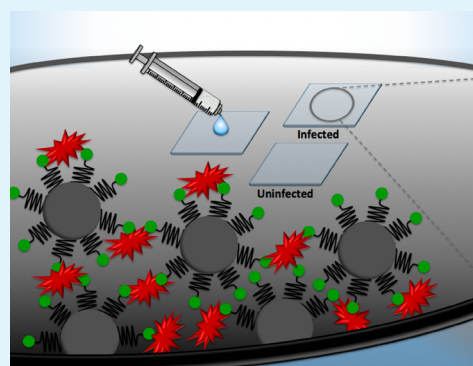
[†]Department of Chemistry, Vanderbilt University, Station B 351822, Nashville, Tennessee 37235-1822, United States

[‡]Department of Biomedical Engineering, Vanderbilt University, Station B 351631, Nashville, Tennessee 37235-1631, United States

S Supporting Information

ABSTRACT: We report a novel, low-resource malaria diagnostic platform inspired by the coffee ring phenomenon, selective for *Plasmodium falciparum* histidine-rich protein-II (PfHRP-II), a biomarker indicative of the *P. falciparum* parasite strain. In this diagnostic design, a recombinant HRP-II (rcHRP-II) biomarker is sandwiched between 1 μm Ni(II)nitrilotriacetic acid (NTA) gold-plated polystyrene microspheres (AuPS) and Ni(II)NTA-functionalized glass. After rcHRP-II malaria biomarkers had reacted with Ni(II)NTA-functionalized particles, a 1 μL volume of the particle–protein conjugate solution is deposited onto a functionalized glass slide. Drop evaporation produces the radial flow characteristic of coffee ring formation, and particle–protein conjugates are transported toward the drop edge, where, in the presence of rcHRP-II, particles bind to the Ni(II)NTA-functionalized glass surface. After evaporation, a wash with deionized water removes nonspecifically bound materials while maintaining the integrity of the surface-coupled ring produced by the presence of the protein biomarker. The dynamic range of this design was found to span 3 orders of magnitude, and rings are visible with the naked eye at protein concentrations as low as 10 pM, 1 order of magnitude below the 100 pM PfHRP-II threshold recommended by the World Health Organization. Key enabling features of this design are the inert and robust gold nanoshell to reduce nonspecific interactions on the particle surface, inclusion of a water wash step after drop evaporation to reduce nonspecific binding to the glass, a large diameter particle to project a large two-dimensional viewable area after ring formation, and a low particle density to favor radial flow toward the drop edge and reduce vertical settling to the glass surface in the center of the drop. This robust, antibody-free assay offers a simple user interface and clinically relevant limits of biomarker detection, two critical features required for low-resource malaria detection.

KEYWORDS: low-resource diagnostics, Ni(II)NTA, polystyrene microspheres, malaria, histidine-rich proteins



1. INTRODUCTION

Robust, inexpensive, and simple diagnostic tests have the potential to improve the quality and efficacy of healthcare in the developing world. Unfortunately, appropriately designed diagnostic tests are often neither available nor affordable. Few tests are optimized for use in low-resource settings where minimal infrastructure, a wide range of environmental conditions (e.g., temperature and humidity), and variable or no access to electricity and clean water are common. For malaria, a disease that threatens 40% of the world's population and kills more than 1 million people per year, antibody-based, immunochromatographic rapid diagnostic tests (RDTs) have been widely deployed for the detection of malarial infection.^{1–3} These devices provide results in as little as 15 min for the detection of *Plasmodium falciparum* antigens such as aldolase, lactate dehydrogenase (LDH), or *Plasmodium falciparum* histidine-rich protein-II (PfHRP-II). Although the primary advantage of RDTs is an extremely simple user interface, a comparative analysis of these strip tests performed under the

auspices of the World Health Organization (WHO) showed troubling variability in performance. In fact, of the 50 RDTs that qualified for the study, only 10% met performance criteria at the WHO's recommended lower limit of detection, 200 parasites/ μL , which corresponds to approximately 0.1–1 nM PfHRP-II in blood.^{1,4–6} The WHO concluded that variance in manufacturing standards and the thermal sensitivity of antibodies were the major causes for performance failure.⁷ As a result, there is a significant need for diagnostic platforms that combine the simple user interface offered by RDTs with stable performance characteristics in those environments commonly encountered in low-resource settings.

Many *P. falciparum* malaria RDT's target PfHRP-II, a 67 kDa protein dimer that contains histidines organized in multiple repeats of AHH and AHHAAD, which comprise 85% of the

Received: September 12, 2013

Accepted: April 14, 2014

Published: April 14, 2014

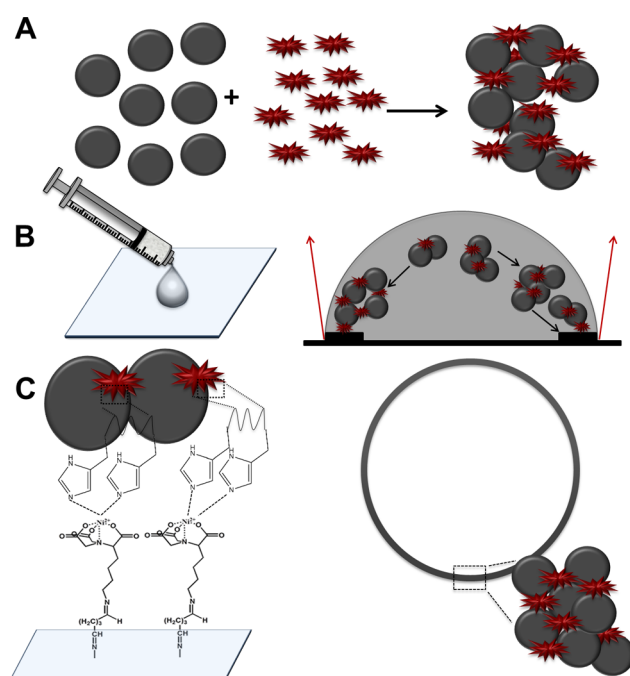
total amino acids.⁸ It is an appealing biomarker because 97% of the protein is released into the host's blood during red blood cell rupture.⁹ We have recently reported a robust Ni(II) nitrilotriacetic acid (NTA) gold nanoparticle (AuNP) sensor specific for peptide mimics of *Pf*HRP-II.¹⁰ In the presence of histidine-rich peptides, the aggregation of Ni(II)NTA AuNPs occurs in as little as 10 min, providing a colorimetric response due to plasmon band coupling.^{11–13} Although the Ni(II)NTA AuNPs are specific toward histidine-rich proteins and false positives are not observed in the presence of various confounding proteins at their respective physiological concentrations, the assay sensitivity does not meet the necessary thresholds to be effective in the field. In addition, a spectrophotometer is required in the Ni(II)NTA AuNP assay to distinguish subtle color changes induced by particle aggregation. In contrast, the ability to concentrate and capture the *Pf*HRP-II biomarker utilizing a robust Ni(II)NTA recognition element in an evaporating drop would not only increase assay sensitivity but also generate a colorimetric ring indicative of the positive presence of the biomarker.

In this report, we describe the design of an antibody-free format for a malaria test based on the everyday phenomenon that forms coffee ring stains on a kitchen counter. As originally described by Deegan and coworkers, evaporating colloidal drops contain an outwardly directed radial flow to replenish solvent that evaporates at a greater rate from the edge of the drop. These radial flows transport materials in solution to the periphery of the drop where they become concentrated and form a characteristic ring pattern.^{14–16} Earlier studies have shown that drying drops containing biological material form patterns with possible applications for separations and diagnostics.^{17–23} We have previously reported an assay design that relies on the coffee ring phenomenon to generate a colorimetric shift in the dried deposition pattern to distinguish between a positive and negative test result.²⁴ In this previous study, magnetic particles (250 nm in diameter) and non-magnetic green particles (1 μm in diameter), both surface-modified with Ni(II)NTA, were shown to bind a poly-L-histidine target, a mimic of the malaria biomarker, *Pf*HRP-II, causing these two different types of particles to form a sandwich. When a drop of this solution was evaporated on plain glass above a magnetic field, these biomarker-induced particle assemblies were immobilized in the center of the drop by the magnetic field, preventing the green particle from migrating to the edge of the drop. Nonreactive red control particles (1 μm diameter) in solution were transported by outwardly directed radial flow to the drop edge and formed a red ring under fluorescence. In the absence of the poly-L-histidine biomarker mimic, both the red and green particles flowed to the edge and created a yellow ring under fluorescence. Therefore, the presence or absence of the biomarker mimic in a water sample created a red or yellow ring upon evaporation of the sample drop, respectively. This previous design has several shortcomings. First, the detection limit of approximately 200 nM must be improved by approximately 3 orders of magnitude to be clinically relevant for malaria detection. Secondly, the design requires the use of a magnetic field to separate particle types during drop evaporation. Finally, the assay does not have a means of eliminating background noise caused by other components in a biological sample, for example red blood cells, which may obstruct the interpretation of the test result.

In this investigation, a simplified enzyme-linked immunosorbent assay (ELISA) format overcomes many of the previous

obstacles by coupling particles to a functionalized glass surface at the edge of an evaporating drop only in the presence of the *Pf*HRP-II malaria biomarker. The design incorporates a unique and robust Ni(II)NTA Au-plated polystyrene microsphere (AuPS) platform and a simple water wash step after evaporation to rinse nonspecific materials from the glass surface, leaving behind a visibly detectable ring indicating a positive test result. Scheme 1 outlines a proposed strategy for

Scheme 1. Proposed Strategy of Ring Formation for rcHRP-II Detection Using Ni(II)NTA AuPSs^a



^a(A) A solution of Ni(II)NTA AuPSs is reacted with rcHRP-II, inducing cross-linking between particles, and ultimately aggregation. (B) A small volume of this particle–protein aggregate solution is deposited onto a Ni(II)NTA-functionalized glass slide (left) and allowed to dry. The right panel shows that evaporation occurs the most rapidly at the edge of the drop (red arrows), so that fluid from the center of the drop migrates to the edge to compensate for the sudden evaporative loss. As a result, a surface tension gradient is created, hereby pulling the particle–protein conjugates toward the edge and forming a ring. (C) After the drop fully dries, the glass is washed with deionized water, and the integrity of the ring is maintained because the rcHRP-II is sandwiched between the Ni(II)NTA-functionalized glass and Ni(II)NTA-functionalized AuNPs, mimicking an enzyme-linked immunosorbent assay. The left panel is a side view upon washing the glass, elucidating the coordination of the histidine residues on rcHRP-II to Ni(II)NTA on the glass. The right panel is a top view, displaying a ring elicited by the formation of aggregated Ni(II)NTA AuPSs.

ring formation in the presence of the malaria biomarker, where recombinant HRP-II (rcHRP-II) is first reacted and sandwiched between Ni(II)NTA AuPSs in solution (Scheme 1A). Next, this biomarker–particle conjugate solution is deposited onto a Ni(II)NTA-functionalized glass slide and allowed to evaporate, where the natural radial flow transports the particles to the drop edge, elucidating a ring (Scheme 1B). The final water rinse step after evaporation maintains the integrity of the ring in the presence of rcHRP-II, whereas nonspecific materials are washed away from the surface. After being rinsed, the

protein biomarker remains sandwiched between the Ni(II)-NTA-functionalized particles and glass slide, elucidating a ring of particles (Scheme 1C). The results presented in this report demonstrate detection of the recombinant malaria biomarker at a clinically relevant limit of detection without the need for an external magnetic field.

2. EXPERIMENTAL SECTION

Materials and Reagents. Ni(II)NTA-functionalized glass was purchased from Xenopore. Amine-terminated polystyrene spheres (1.1 μm) were purchased from Life Technologies Corp. Recombinant *P. falciparum* histidine-rich protein-II containing a glutathione S-transferase (GST) fusion tag was obtained from CTK Biotech. Human serum albumin (HSA), GST, and α_2 -macroglobulin (A2M) were purchased from Sigma-Aldrich. Thiol-dPEG₄-acid was purchased from Quanta Bioscience. *N*-Cyclohexyl-2-aminoethanesulfonic acid (CHES) and 2-(*N*-morpholino)ethanesulfonic acid (MES) buffers were purchased from Sigma. All other reagents are of analytical grade and used as received from either Sigma-Aldrich or Fisher Scientific. Ultrapure water with a resistivity of $>18\text{ M}\Omega\text{ cm}$ was used for all experiments.

Instrumentation. Transmission electron microscopy (TEM) images were captured using a Phillips CM20 microscope at 200 kV. Size distributions of suspended particles were determined by dynamic laser scattering (DLS) using a Malvern Nano Zetasizer. Spectral characterization was performed on either an Agilent 8453 UV-vis spectrophotometer or a Bio-Tek Synergy H4 plate reader. Ring images were captured with a 2 \times objective on a Nikon TE2000U inverted microscope with a charge-coupled device (CCD) camera (Hamamatsu Photonics, model C7780-20).

Synthesis of THPC-Functionalized AuNP Seeds. Tetrakis-(hydroxymethyl)phosphonium chloride (THPC)-functionalized AuNPs (2–4 nm) were synthesized in a 100 mL round bottom flask by combining 500 μL of 1 M NaOH and 1 mL of 0.95% (v/v) THPC with 45 mL of deionized (DI) H₂O. To the vigorously stirred solution was rapidly added 10 mL of 5 mM HAuCl₄, changing the color from clear to dark brown in seconds. The solution was stirred for an additional 1 min, and the pH was decreased to 5.5 with concentrated hydrochloric acid.

Synthesis of Au-Plated Polystyrene Microspheres (AuPSs). The plating of gold nanoshells, first pioneered by Halas et al., has been subsequently modified to accommodate 1 μm polystyrene spheres.^{25–29} A seed-mediated adsorption onto polystyrene was achieved by combining a 5 mL solution of stock THPC-functionalized AuNPs (pH 5.5) with a 25 μL stock solution (45 pM) of washed amine-terminated polystyrene microspheres. After being stirred vigorously for 24 h, the solution was centrifuged at 1200g (3400 rpm) for 10 min. The polystyrene spheres were washed by decanting the AuNP supernatant and suspending in 5 mL of H₂O. This process was repeated four additional times, in which the final volume of the AuNP-seeded polystyrene particle suspension was 25 μL in H₂O. To achieve a uniform gold nanoshell encompassing the polystyrene microsphere, an electroless plating solution was first prepared separately by dissolving 50 mg of K₂CO₃ in 185 mL of DI H₂O and stirring for 5 min. Next, 15 mL of 5 mM HAuCl₄ was added to the solution, and stirring was ceased. Over the course of 30 min, the solution turned from light yellow to clear, indicating the reduction of Au(III) to Au(I). This solution was aged overnight in the dark to prevent photocatalytic reduction of Au(I) to Au(0). In a conical tube, 25 μL of the AuNP-seeded polystyrene spheres was suspended in 5 mL of the aged electroless plating solution before the addition of 10 μL of 37% formaldehyde to promote the reduction of Au(I) onto the AuNPs adsorbed to polystyrene. This solution was vortexed for 2 min and subsequently turned black, indicating the plating of a thin gold nanoshell encompassing the polystyrene. Next, the 5 mL of solution was centrifuged for 5 min at 1200g. The supernatant was then decanted, and the Au-plated particles were suspended in 3 mL of DI H₂O. The centrifugation process was repeated three additional times

before suspension in 1 mL of DI H₂O to achieve a particle concentration of 1 pM.

Synthesis of Ni(II)NTA AuPSs. To achieve a Ni(II)NTA recognition platform, 5 mM thiol-dPEG₄-acid was mixed with 5 mM of a modular, thiolated NTA ligand that was previously synthesized in our lab.¹⁰ To the 1 pM Au-plated polystyrene suspension was added 10 μL (100 μM total ligand) of the ligand solution and the mixture incubated overnight. Three washes were performed by centrifuging the particles at 1200g for 5 min and resuspending in 3 mL of water. The NTA-functionalized particles were suspended in 1 mL of 0.1 M CHES buffer (pH 9.0), and 100 μM NiCl₂·6H₂O was added. The particles were incubated overnight and subsequently washed four times at 1200g for 5 min with water.

Quantifying Gold Concentrations on AuPSs. To quantify the average gold concentration on each polystyrene particle, 100 μL aliquots of 1 pM suspensions of AuNP-seeded polystyrene particles and NH₂-terminated polystyrene spheres were treated with 400 μL of 8 mM KCN and agitated for 15 min. Next the particles were centrifuged at 16100g for 5 min, and the supernatant was decanted and finally filtered through a 0.22 μm filter. The UV spectrum of the K[Au(CN)₂] complex has known extinction coefficients at 204, 211, 230, and 240 nm.^{30,31} To quantify the average gold concentration on each AuPS, a 50 μL aliquot of a 1 pM suspension of AuPSs was treated with 450 μL of 8 mM KCN and agitated for 15 min. Next the particles were centrifuged at 16100g for 5 min, and the supernatant was then decanted and filtered through a 0.22 μm filter. The UV spectrum of the K[Au(CN)₂] complex was then measured with an Agilent 8453 spectrophotometer.

Dynamic Laser Light Scattering Assays with Ni(II)NTA AuPSs. A 90 μL aliquot of 1 pM Ni(II)NTA AuPSs suspended in 0.1 M MES buffer containing 125 mM imidazole and 0.02% Tween 20 (pH 5.5) was reacted against 10 μL of a protein solution for 15 min. Afterward, size distribution profiles of the particles were taken; an average hydrodynamic particle diameter was conferred.

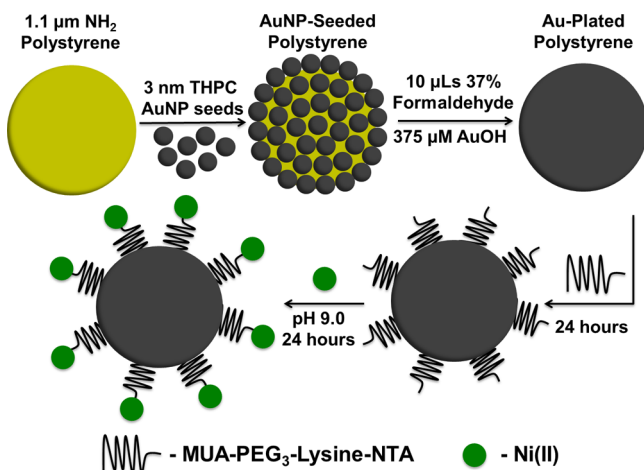
Ring Assays with Ni(II)NTA AuPSs. Ni(II)NTA AuPS (1 pM) containing 0.02% Tween 20 were reacted against varying concentrations of rCHRP-II and GST for 15 min at pH 5.5. Afterward, 1% glycerol was added to the solution, and a 1 μL suspension of the microsphere–protein conjugate was pipetted onto a Ni(II)NTA glass slide and allowed to evaporate for 1 h, yielding a total assay time of 75 min. Afterward, the glass slides were rinsed thoroughly with water, and the glass was subsequently imaged with Image Pro Plus (version 7).

Ring Image Analysis. The distribution of the Ni(II)NTA particle aggregates in evaporated droplets is analyzed using Image Pro Plus (version 7) processing software by representing the AuNPs within the image as positive pixel density or signal intensity. Background noise is determined by measuring intensity in four predefined areas of interest (AOI) at the corner of each image. Signal intensity is measured with two concentric, predefined AOIs: an outer AOI that includes the entire drop and an inner AOI centered inside the drop. After background noise is subtracted, the ring annulus intensity is calculated by subtracting the inner AOI from the outer AOI. The signal, defined as the presence of a ring, is calculated by dividing the ring annulus intensity by the ring annulus intensity of the blanks. Signal values are normalized so a value of 1 corresponds to minimal ring formation.

3. RESULTS

Synthesis of AuPSs. The microparticle synthesis begins with a seed-mediated approach by first electrostatically adsorbing 2–4 nm THPC-functionalized AuNPs onto amine-terminated polystyrene microspheres, followed by reducing Au(I) onto the adsorbed AuNPs with the reducing agent, formaldehyde (Scheme 2). The subsequent oxidation and dehydrogenation of formaldehyde are facilitated in the presence of a catalytic metal such as gold,³² so that the product is a tailored, thin gold nanoshell encompassing the polystyrene. When the amine-terminated polystyrene spheres react with THPC-functionalized AuNPs, the color of the solution changes

Scheme 2. Synthesis of Ni(II)NTA AuPSs



slightly from bright to dark yellow, and TEM images display the THPC-functionalized AuNP seeds adsorbed to the surface of the amine-terminated microspheres (Figure 1A,B). AuNP-

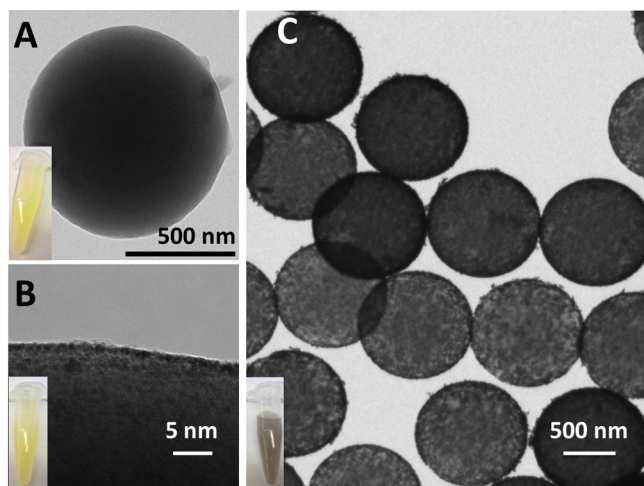


Figure 1. Characterization of AuPSs upon addition of AuNP seeds and Au plating. TEM images of (A) an amine-terminated polystyrene sphere, (B) the surface of a polystyrene sphere with adsorbed 2–4 nm AuNPs, and (C) Au-plated polystyrene spheres (AuPSs). The insets at the bottom left of each panel show the color of a 1 pM aliquot of each type of microsphere.

seeded polystyrene spheres then undergo an electroless plating deposition in the presence of AuOH, where TEM images reveal a thin gold nanoshell encompassing the polystyrene (Figure 1C). There is an average of 8.3×10^8 total Au atoms/particle, as determined by UV–vis spectroscopy, equating to an average density of 1.49 g/mL and an average particle settling velocity of 3.2×10^{-5} cm/s (Supporting Information).

Aggregation Assays with Ni(II)NTA AuPSs. The modular thiol-peg-Ni(II)NTA ligand provides an ideal, validated recognition element to create the particle–biomarker capture interface.¹⁰ Upon functionalization with this Ni(II)NTA recognition element, the particles are stable and monodisperse, as shown by TEM images (Figure 2A). When the Ni(II)NTA AuPSs are reacted with rcHRP-II at pH 5.5, significant aggregation is first observed at high rcHRP-II concentrations via Ni(II)–histidine cross-linking between

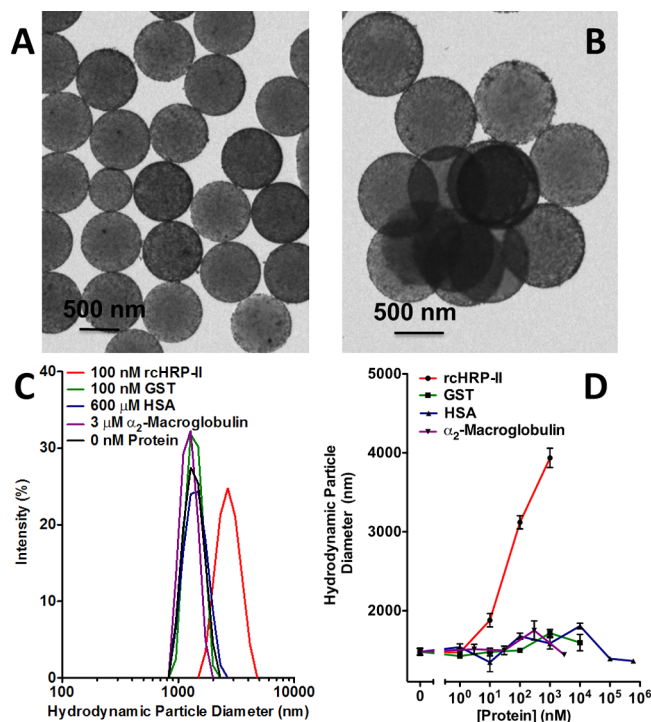


Figure 2. Activity and specificity of Ni(II)NTA AuPSs. TEM images of Ni(II)NTA AuPSs (A) before and (B) after addition of 1 μM rcHRP-II. (C) Dynamic laser light scattering size distribution profiles of Ni(II)NTA AuPSs in the presence of various confounding proteins at their respective physiological concentrations. (D) Titrations of rcHRP-II in addition to confounding proteins as measured by dynamic laser light scattering.

rcHRP-II and the particles, as shown by TEM images and dynamic laser light scattering experiments (Figure 2B–D). Dynamic laser light scattering also validates the specificity of the molecular recognition interface toward the biomarker, as a shift in the size distribution of the Ni(II)NTA AuPSs is insignificant when they react at the physiological concentrations of HSA (40 mg/mL) and α_2 -macroglobulin (A2M, 2 mg/mL) (Figure 2C,D). Controls against the fusion protein, glutathione S-transferase (GST), showed no aggregation, highlighting the specificity of the Ni(II)NTA molecular recognition element toward the biomarker.

Ring Assays with a 1.1 μm Ni(II)NTA AuPS Platform. Subsequently, the Ni(II)NTA AuPSs are evaluated in the coffee ring assay. After incubation of the Ni(II)NTA AuPSs with rcHRP-II for 15 min, the particle–protein conjugate solution is spotted onto a Ni(II)NTA-functionalized glass slide, and the drop edge is pinned to the glass surface via topographical and chemical heterogeneities. As the extent of evaporation is greatest at the drop edge, solution from the middle of the drop migrates toward the contact line to compensate for the rapid fluid loss. Suspended Ni(II)NTA AuPS–protein conjugates flow radially toward the drop edge and accumulate at the contact line, as shown by images of a drop of particles at different time points during evaporation (Supporting Information). When rcHRP-II is present, the particles are captured by the functionalized glass surface. Rinsing the glass slide with deionized water after depositing and evaporating 1 μL of a AuPS–protein conjugate solution washes away nonspecific binding on the surface. At 10 nM rcHRP-II, the integrity of the ring is maintained via conjugate coupling to the Ni(II)NTA

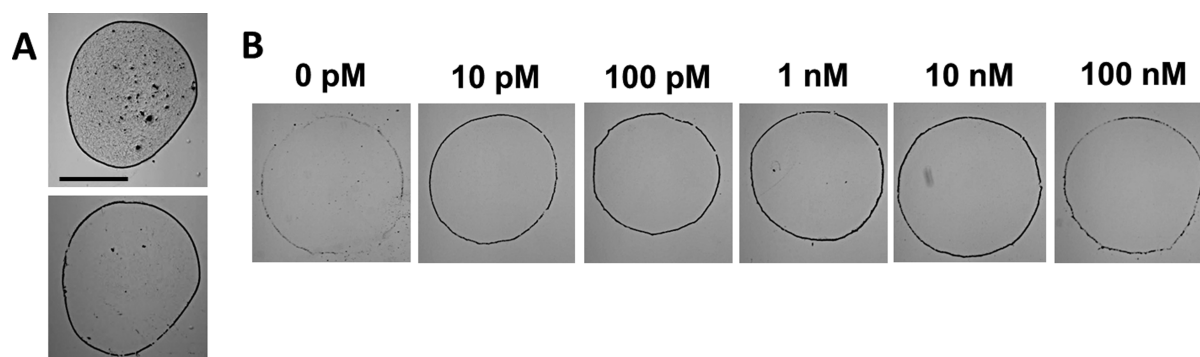


Figure 3. Ni(II)NTA AuPS ring assay for detection of rCHRP-II. (A) A 1 pM solution of Ni(II)NTA AuPSs containing 0.02% Tween and 1% glycerol is reacted with 10 nM rCHRP-II, and a 1 μ L drop is deposited on a Ni(II)NTA-functionalized glass slide. After 1 h, the slide is rinsed thoroughly with deionized water. The top image shows the drop before washing, while the bottom image shows the drop after washing in the presence of the rCHRP-II biomarker. The black bar is 1 mm. (B) Logarithmic titration of rCHRP-II using the conditions described above. The images show an example of the rings after washing.

glass surface (Figure 3A). In the presence of rCHRP-II, the polystyrene spheres exhibit ring formation over a titration range of 3 orders of magnitude of the target biomarker (Figure 3B). The titration of rCHRP-II with Ni(II)NTA AuPSs exhibits an optical detection limit of 10 pM rCHRP-II. The assay signal intensity increases linearly after 10 pM rCHRP-II before saturating between 100 pM and 10 nM. In the high-concentration regime of the assay, 100 nM rCHRP-II concentrations aggregate the particles, so that the protein–particle conjugates settle vertically (6.0×10^{-5} cm/s) to the center of the drop rather than radially flowing toward the edge upon drop deposition. Upon being washed, the large aggregates are displaced, as there is not enough particle surface area contact with the Ni(II)NTA glass to coordinate the particle–protein conjugates to the surface, resulting in faint rings. Image processing further allows for quantitation and validation of the assay, as indicated by a titration curve between 10 pM and 10 nM rCHRP-II (Figure 4). The fusion protein, GST, is used to

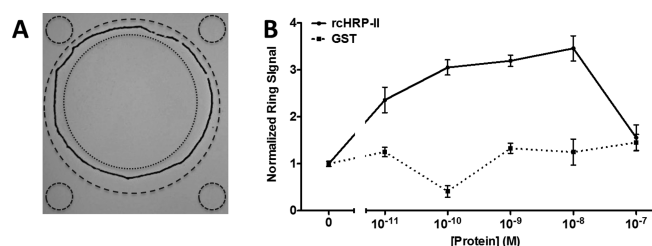


Figure 4. Analysis of ring formation from the titration of rCHRP-II with Ni(II)NTA AuPSs. (A) Ring signal generated by subtracting the intensity of the inner circularly dotted annulus from the outer dashed annulus with respect to the minimal mean background (four dashed corner circles). The solid ring in the image is an example of concentrated Ni(II)NTA AuPSs in a ring in the presence of rCHRP-II after washing. (B) Compiled signal intensity generated from the difference between the dotted annulus inside the ring with from the dashed outer annulus with respect to the minimal mean background signal.

control for nonspecific interactions. Particle aggregation does not occur in the presence of GST, and the ring signal generated upon reactions with GST does not exceed the background noise.

4. DISCUSSION

This simple antibody-free design originally inspired by the coffee ring phenomenon overcomes many of the obstacles associated with existing RDTs by manipulating the molecular recognition interface for optimal specificity and improved sensitivity. The ring assay simplifies an ELISA by eliciting a chromogenic response from concentrated polystyrene microspheres. In our low-resource design, a ring of Ni(II)NTA AuPSs sandwich a rCHRP-II malarial biomarker with Ni(II)-NTA-functionalized glass via Ni(II)–histidine coordination. Most importantly, the integration of a water wash step after drop evaporation significantly reduces nonspecific binding to the glass surface but maintains the integrity of the strong Ni(II)–histidine coordination in the presence of the biomarker. This assay detects biomarker concentrations over the operational range of malaria diagnostics (0.1–1 nM rCHRP-II) recommended by the WHO, and rings are even visible with the naked eye at 10 pM rCHRP-II. This 10 pM viewable limit of detection is 1 order of magnitude below the WHO’s lower recommended threshold concentration, so that our format possesses utility diagnosing malaria in asymptomatic patients. In the high-concentration regime, the assay’s ring signal decreases because of particle aggregation and gravitational vertical settling to the center of the drop.³³ However, it has been determined that for adults and children infected with uncomplicated and severe malaria, the median concentration of *Pf*HRP-II found in blood is between 1 and 10 nM,^{5,34,35} which is the most sensitive regime of our assay.

To achieve a detection limit below 0.1 nM *Pf*HRP-II using a microfluidic ring assay, an aqueous polystyrene microsphere is a desirable particle platform because of the high degree of uniformity, the low density, and the large particle surface area. The low density of the spherical, monodisperse particle favors ring formation, while the large surface area creates a viewable two-dimensional ring that provides the assay’s signal. A spherical, monodisperse bead also provides reproducible and predictable particle flow in evaporating drops, so the assay can be easily tuned and manipulated. In addition, coating the polystyrene particle in a gold nanoshell to promote facile thiol-based ligand functionalization offers a robust interface, which can withstand the extreme conditions encountered in low-resource areas. Finally, this inert gold nanoshell minimizes nonspecific interactions and validates the integrity of our

previously explored Ni(II)NTA AuNP molecular recognition interface.¹⁰

The introduction of the additives, Tween and glycerol, enhances particle stability, reproducible particle flow, and the signal-to-noise ratio. It has been previously demonstrated that the incorporation of surfactants and polymers into particle droplet suspensions can promote and prevent ring formation during drop evaporation.^{36–38} Manipulating such factors leads to improved ring reproducibility and robustness by controlling the rate of evaporation and blocking nonspecific substrate binding. In this format, incorporating 0.02% Tween 20 into the particle suspension maintains particle stability, while aiding in contact line pinning during drop evaporation for reproducible ring sizes. Additionally, the incorporation of 1% glycerol not only promotes specific Ni(II)–histidine coordination to the glass but also provides adequate blocking on the functionalized glass surface to limit nonspecific binding. In contrast to an ELISA in which proteins are often used to block nonspecific sites, our assay takes advantage of the robust hydrogen bonding network of glycerol and/or water as a blocking agent, further modifying this assay for use in low-resource areas. Finally, the viscous nature of glycerol reduces the rate of evaporation to optimize the kinetics of transport of the particle to the drop edge for an increased signal.

5. CONCLUSIONS

The coffee ring-inspired diagnostic strategy described in this work delivers a unique approach for overcoming challenges associated with existing rapid diagnostic tests, particularly in low-resource settings. Enabled by the stable Au–thiol interface and the monodisperse, spherical distribution of colloidal gold nanoparticles, rings of 1 μm Ni(II)NTA AuPSs detect concentrations of the rCHRP-II malarial biomarker as low as 10 pM, 1 order of magnitude lower than current diagnostic standards. The inert gold surface provides a stable and selective Ni(II)NTA molecular recognition element toward rCHRP-II that resists the extreme conditions in low-resource regions. The assay offers a simple user interface through complementary Ni(II)–histidine coordination on the glass surface, where the signal is enhanced significantly by reducing background noise with a final water wash. The overall assay performance is additionally enhanced through the judicious use of additives. Furthermore, applying the image processing algorithms upon ring identification to cell phone technology has the potential to further enhance the simple user interface and reduce user bias in low-resource settings.³⁹ Finally, the assay time required to generate positive or negative results is comparable to currently available RDTs, so that coupling this format to a self-contained extraction device⁴⁰ specific for PfHRP-II from a whole blood matrix would greatly facilitate the sample preparation to operate as a malarial diagnostic.

■ ASSOCIATED CONTENT

■ Supporting Information

Synthesis and characterization of the AuNP seeds, calculation of the AuPS average particle density, dynamic laser light scattering spectral profiles of Ni(II)NTA AuPSs upon their reaction with varying confounding proteins at their respective physiological concentrations, images showing the progression of Ni(II)NTA AuPS drying on Ni(II)NTA glass, glycerol optimization, drying time optimization, and prewash characterization of Ni(II)NTA AuPSs adsorbed to glass. This material is available free of charge via the Internet at <http://pubs.acs.org>.

■ AUTHOR INFORMATION

Corresponding Authors

*E-mail: rick.haselton@vanderbilt.edu. Fax: (615) 343-7919. Telephone: (615) 322-6622.

*E-mail: david.wright@vanderbilt.edu. Fax: (615) 343-1234. Telephone: (615) 322-2636.

Notes

The authors declare no competing financial interest.

■ ACKNOWLEDGMENTS

This research was supported in part by the Bill and Melinda Gates Foundation and a Vanderbilt University Discovery Grant. We thank M. F. Richards for critical comments concerning the manuscript.

■ REFERENCES

- (1) Martin, S. K.; Rajasekariah, G. H.; Awinda, G.; Waitumbi, J.; Kifude, C. Unified Parasite Lactate Dehydrogenase and Histidine-Rich Protein ELISA for Quantification of *Plasmodium falciparum*. *Am. J. Trop. Med. Hyg.* **2009**, *80*, 516–522.
- (2) Quintana, M.; Piper, R.; Boling, H. L.; Makler, M.; Sherman, C.; Gill, E.; Fernandez, E.; Martin, S. Malaria Diagnosis by Dipstick Assay in a Honduran Population with Coendemic *Plasmodium falciparum* and *Plasmodium vivax*. *Am. J. Trop. Med. Hyg.* **1998**, *59*, 868–871.
- (3) Singh, N.; Saxena, A.; Valecha, N. Field Evaluation of the ICT Malaria P.f/P.v Immunochromatographic Test for Diagnosis of *Plasmodium falciparum* and *P. vivax* Infection in Forest Villages of Chhindwara, Central India. *Trop. Med. Int. Health* **2000**, *5*, 765–770.
- (4) Minigo, G.; Woodberry, T.; Piera, K. A.; Salwati, E.; Tjitra, E.; Kenangalem, E.; Price, R. N.; Engwerda, C. R.; Anstey, N. M.; Plebanski, M. Parasite-Dependent Expansion of TNF Receptor II-Positive Regulatory T Cells with Enhanced Suppressive Activity in Adults with Severe Malaria. *PLoS Pathog.* **2009**, *5*, e1000402.
- (5) Dondorp, A. M.; Desakorn, V.; Pongtavornpinyo, W.; Sahassananda, D.; Silamut, K.; Chotivanich, K.; Newton, P. N.; Pitisuttithum, P.; Smithyman, A. M.; White, N. J.; Day, N. P. J. Estimation of the Total Parasite Biomass in Acute *Falciparum* Malaria from Plasma PfHRP2. *PLoS Med.* **2005**, *2*, e204.
- (6) Kifude, C. M.; Rajasekariah, G. H.; Sullivan, D. J., Jr.; Stewart, V. A.; Angov, E.; Martin, S. K.; Diggs, C. L.; Waitumbi, J. N. Enzyme-Linked Immunosorbent Assay for Detection of *Plasmodium falciparum* Histidine-Rich Protein 2 in Blood, Plasma, and Serum. *Clin. Vaccine Immunol.* **2008**, *15*, 1012–1018.
- (7) World Malaria Report; World Health Organization: Geneva, 2011.
- (8) Panton, L. J.; McPhie, P.; Maloy, W. L.; Wellems, T. E.; Taylor, D. W.; Howard, R. Purification and Partial Characterization of an Unusual Protein of *Plasmodium falciparum*: Histidine-Rich Protein II. *Mol. Biochem. Parasitol.* **1989**, *35*, 149–160.
- (9) Chiodini, P. L.; Bowers, K.; Jorgensen, P.; Barnwell, J. W.; Grady, K. K.; Luchavez, J.; Moody, A. H.; Cenizal, A.; Bell, D. The Heat Stability of *Plasmodium* Lactate Dehydrogenase-Based and Histidine-Rich Protein 2-Based Malaria Rapid Diagnostic Tests. *Trans. R. Soc. Trop. Med. Hyg.* **2007**, *101*, 331–337.
- (10) Swartz, J. D.; Gulka, C. P.; Haselton, F. R.; Wright, D. W. Development of Histidine-Targeted Spectrophotometric Sensor Using Ni(II)NTA-Functionalized Au and Ag Nanoparticles. *Langmuir* **2011**, *27*, 15330–15339.
- (11) Kreibig, U.; Genzel, L. Optical Absorption of Small Metallic Particles. *Surf. Sci.* **1985**, *156*, 678–700.
- (12) Quinten, M.; Kreibig, U. Optical Properties of Aggregates of Small Metal Particles. *Surf. Sci.* **1986**, *172*, 557–577.
- (13) Prodan, E.; Nordlander, P. Plasmon Hybridization in Spherical Nanoparticles. *J. Chem. Phys.* **2004**, *120*, 5444–5454.
- (14) Deegan, R. D.; Bakajin, O.; Dupont, T. F.; Huber, G.; Nagel, S. R.; Witten, T. A. Capillary Flow as the Cause of Ring Stains from Dried Liquid Drops. *Nature* **1997**, *389*, 827–829.

- (15) Deegan, R. D. Pattern Formation in Drying Drops. *Phys. Rev. E* **2000**, *61*, 475–485.
- (16) Deegan, R. D.; Bakajin, O.; Dupont, T. F.; Huber, G.; Nagel, S. R.; Witten, T. A. Contact Line Deposits in an Evaporating Drop. *Phys. Rev. E* **2000**, *62*, 756–765.
- (17) Tarasevich, Y. Y.; Pravoslavnova, D. M. Segregation in Desiccated Sessile Drops of Biological Fluids. *Eur. Phys. J. E: Soft Matter Biol. Phys.* **2007**, *22*, 311–314.
- (18) Tarasevich, Y. Y.; Pravoslavnova, D. M. Drying of a Multicomponent Solution Drop on a Solid Substrate: Qualitative Analysis. *Technol. Phys.* **2007**, *52*, 159–163.
- (19) Larson, R. G.; Lopez, M. A.; Lim, D. W.; Lahann, J. Complex Protein Patterns in Drying Droplets. *MRS Proceedings* **2010**, 1273.
- (20) Brutin, D.; Sobac, B.; Loquet, B.; Sampol, J. Pattern Formation in Drying Drops of Blood. *J. Fluid Mech.* **2011**, *667*, 85–95.
- (21) Wong, T. S.; Chen, T. H.; Shen, X. Y.; Ho, C. M. Nanochromatography Driven by the Coffee Ring Effect. *Anal. Chem.* **2011**, *83*, 1871–1873.
- (22) Wen, J. T.; Ho, C. M.; Lillehoj, P. B. Coffee Ring Aptasensor for Rapid Protein Detection. *Langmuir* **2013**, *29*, 8440–8446.
- (23) Trantum, J. R.; Baglia, M. L.; Eagleton, Z. E.; Mernaugh, R. L.; Haselton, F. R. Biosensor Design Based on Marangoni Flow in an Evaporating Drop. *Lab Chip* **2014**, *14*, 315–324.
- (24) Trantum, J. R.; Wright, D. W.; Haselton, F. R. Biomarker-Mediated Disruption of Coffee-Ring Formation as a Low Resource Diagnostic Indicator. *Langmuir* **2012**, *28*, 2187–2193.
- (25) Westcott, S. L.; Oldenburg, S. J.; Lee, T. R.; Halas, N. J. Formation and Adsorption of Clusters of Gold Nanoparticles onto Functionalized Silica Nanoparticle Surfaces. *Langmuir* **1998**, *14*, 5396–5401.
- (26) Oldenburg, S. J.; Averitt, R. D.; Westcott, S. L.; Halas, N. J. Nanoengineering of Optical Resonances. *Chem. Phys. Lett.* **1998**, *288*, 243–247.
- (27) Pham, T.; Jackson, J. B.; Halas, N. J.; Lee, T. R. Preparation and Characterization of Gold Nanoshells Coated with Self-Assembled Monolayers. *Langmuir* **2002**, *18*, 4915–4920.
- (28) Shi, W.; Sahoo, Y.; Swihart, M. T.; Prasad, P. N. Gold Nanoshells on Polystyrene Cores for Control of Surface Plasmon Resonance. *Langmuir* **2005**, *21*, 1610–1617.
- (29) Piao, L.; Park, S.; Lee, H. B.; Kim, K.; Kim, J.; Chung, T. D. Single Gold Microshell Tailored to Sensitive Surface Enhanced Raman Scattering Probe. *Anal. Chem.* **2010**, *82*, 447–451.
- (30) Knecht, M. R.; Wright, D. W. Dendrimer Mediated Formation of Multicomponent Nanospheres. *Chem. Mater.* **2004**, *16*, 4890–4895.
- (31) Perumareddi, J. R.; Liehr, A. D.; Adamson, A. W. Ligand Field Theory of Transition Metal Cyanide Complexes. Part I. The Zero, One and Two Electron or Hole Configurations. *J. Am. Chem. Soc.* **1963**, *85*, 249–259.
- (32) Van Den Meerakker, J. E. A. M. On the Mechanism of Electroless Plating. II. One Mechanism for Different Reductants. *J. Appl. Electrochem.* **1981**, *11*, 395–400.
- (33) Trantum, J. R.; Eagleton, Z. E.; Patil, C. A.; Tucker-Schwartz, J. M.; Baglia, M. L.; Skala, M. C.; Haselton, F. R. Cross-Sectional Tracking of Particle Motion in Evaporating Drops: Flow Fields and Interfacial Accumulation. *Langmuir* **2013**, *29*, 6221–6231.
- (34) Manning, L.; Laman, M.; Stanisic, D.; Rosanas-Urgell, A.; Bona, C.; Teine, D.; Siba, P.; Mueller, I.; Davis, T. M. E. Plasma *Plasmodium falciparum* Histidine-Rich Protein-2 Concentrations Do Not Reflect Severity of Malaria in Papua New Guinean Children. *Clin. Infect. Dis.* **2011**, *52*, 440–446.
- (35) Rubach, M. P.; Mukemba, J.; Florence, S.; John, B.; Crookston, B.; Lopansri, B. K.; Yeo, T. W.; Piera, K. A.; Alder, S. C.; Weinberg, J. B.; Anstey, N. M.; Granger, D. L.; Mwaikambo, E. D. Plasma *Plasmodium falciparum* Histidine-Rich Protein-2 Concentrations Are Associated with Malaria Severity and Mortality in Tanzanian Children. *PLoS One* **2012**, *7*, e35985.
- (36) Vyawahare, S.; Craig, K. M.; Scherer, A. Patterning Lines by Capillary Flows. *Nano Lett.* **2006**, *6*, 271–276.
- (37) Still, T.; Yunker, P. J.; Yodh, A. G. Surfactant-Induced Marangoni Eddies Alter the Coffee-Rings of Evaporating Colloidal Drops. *Langmuir* **2012**, *28*, 4984–4988.
- (38) Cui, L.; Zhang, J.; Zhang, X.; Huang, L.; Wang, Z.; Li, Y.; Gao, H.; Zhu, S.; Wang, T.; Yang, B. Suppression of the Coffee Ring Effect by Hydrosoluble Polymer Additives. *ACS Appl. Mater. Interfaces* **2012**, *4*, 2775–2780.
- (39) Prue, C. S.; Shannon, K. L.; Khyang, J.; Edwards, L. J.; Ahmed, S.; Ram, M.; Shields, T.; Hossain, M.; Glass, G. E.; Nyunt, M. M.; Sack, D. A.; Sullivan, D. A., Jr.; Khan, W. A. Mobile Phones Improve Case Detection and Management of Malaria in Rural Bangladesh. *Malar. J.* **2013**, *12*, 48–54.
- (40) Davis, K. M.; Swartz, J. D.; Haselton, F. R.; Wright, D. W. Low-Resource Method for Extracting the Malarial Biomarker Histidine-Rich Protein II to Enhance Diagnostic Test Performance. *Anal. Chem.* **2012**, *84*, 6136–6142.